Acta Crystallographica Section C
Crystal Structure Communications
ISSN 0108-2701

Poly[tetrakis(*n*-propylammonium) [octa-μ-chlorido-dichloridotrinickelate(II)]]: a hybrid organic–inorganic layer compound in the $Cs_4Mg_3F_{10}$ structure type

Allison Talley, Annette F. Kelley and Marcus R. Bond*

Department of Chemistry, Southeast Missouri State University, Cape Girardeau, MO 63701, USA
Correspondence e-mail: mbond@semo.edu

Received 19 October 2011
Accepted 22 November 2011
Online 30 November 2011

The title compound, $\{(C_3H_{10}N)_4[Ni_3Cl_{10}]\}_n$, contains zigzag layers of tri-μ-chlorido-bridged linear 2/*m*-symmetric Ni_3Cl_{12} segments, linked by mono-μ-chlorido quasi-linear bridges to two other segments at each end. These inorganic layers are interleaved with interdigitated bilayers of mirror-symmetric *n*-propylammonium cations, the ammonium head groups of which are directed into the inorganic layers to form multiple N—H···Cl hydrogen bonds, while the propyl tail groups pack together in a tongue-and-groove manner in the center of the bilayer. The propyl groups are ordered at 100 K but disordered with opposite conformations on the mirror plane at 240 K.

Comment

Layered organic–inorganic hybrid materials are of interest for electrical and optical device applications (Mitzi *et al.*, 2001; Mitzi, 2004). Among these are A_2MX_4 layer perovskites (*A* = organic cation, *M* = metal cation and *X* = monatomic anion), descended from the parent K_2NiF_4 structure, in which layers of corner-sharing MX_6 octahedra are interleaved with bilayers of organic cations (Maxcy & Willett, 2004). The organic bilayers are typically composed of *n*-alkylammonium or anilinium cations in which the $-NH_3$ head group fits into the inorganic layer so as to form hydrogen bonds with the anions, while the nonpolar tails of the cations project into the center of the bilayer. Layer perovskites are also a source for the study of structural phase transitions, often involving progressive disorder of the organic cation, of which a prominent example is the sequence of six different phases in $(n\text{-}C_3H_7NH_3)_2[MnCl_4]$ [Depmeier, 2009, and references therein; Cambridge Structural Database (CSD, Version 5.32; Allen, 2002) refcodes PAMMNC01–17, 26, and 36].

Dussarrat *et al.* (1995) have examined structures derived from K_2NiF_4 through crystallographic shears. Among these is the $Ba_4(Ti,Pt)_3O_{10}$ structure (Blattner *et al.*, 1948), consisting of trimetal segments of face-sharing MO_6 octahedra bridged through corner-sharing to two other segments at each end to establish a zigzag layer in the *ac* plane of the orthorhombic *Cmce* unit cell. The zigzag layer is derived from the parent K_2NiF_4 structure by dividing the $(NiF_4^{2-})_n$ network layer into slabs two NiF_6 complexes wide. Alternate slabs are displaced perpendicular to the layer plane to a point approximately midway between the layers, with F^- ions added to maintain full Ni^{2+} coordination, and with small lateral displacements of the slabs to give regular octahedral holes between slabs from neighboring layers. Additional Ni^{2+} cations are then positioned in these octahedral holes to generate the trimetal segments of face-sharing NiF_6 octahedra. Inorganic $A_4M_3X_{10}$ compounds with this structure type are well known and typically occur when *A* is a large group IA or IIA metal cation and *X* is a small anion, *e.g.* F^-, O^{2-} or H^-. $Cs_4Mg_3F_{10}$ (Steinfink & Brunton, 1969) is also used to identify the aristotype structure, with further examples, such as $Ba_4Ir_3O_{10}$ (Wilkens & Müller-Buschbaum, 1991), $Ba_4(Ir,Al)_3O_{10}$ (Müller-Buschbaum & Neubacher, 1990; Neubacher & Müller-Buschbaum, 1991), $Cs_4M'_3F_{10}$ (*M*′ = Co, Ni or Zn; Schmidt *et al.*, 1992), $Ba_4Ru_3O_{10}$ (Dussarrat *et al.*, 1996; Carim *et al.*, 2000), $Sr_4Mn_3O_{10}$ (Floros *et al.*, 2000) and $Cs_4Mg_3H_{10}$ (Bertheville *et al.*, 2002), illustrating the range of this structure type. A related structure is exemplified by $Cs_4Cu_3F_{10}$, in which linear tricopper segments of face-sharing CuF_6 octahedra are likewise bridged through corner-sharing to two other segments at each end, but in a stepwise fashion so that the terminal ligands on neighboring corner-shared CuF_6 octahedra are *trans*, rather than *cis* as in the $Cs_4Mg_3F_{10}$-type structures (Kissel & Hoppe, 1988; Dussarrat *et al.*, 1995).

Over the past two decades, several examples of hybrid organic–inorganic compounds in the $Cs_4Mg_3F_{10}$ structure type have been identified. First reported was the structure of $(C_6H_5NH_3)_4[Cd_3Br_{10}]$ (Ishihara *et al.*, 1994; CSD refcode POPHAD); the isomorphous chloride structure is more recent (Costin-Hogan *et al.*, 2008; EGUFUI). The structures of two $[Pb_3I_{10}]^{4-}$ salts, *viz.* $C_6H_5CH_2SC(NH_2)_2^+$ (Raptopoulou *et al.*, 2002; IGECIG) and $C_6H_5(CH_2)_3NH_3^+$ (Billing & Lemmerer, 2006*a*; WEHSAE), followed. $(i\text{-}C_3H_7NH_3)_4[Cd_3Cl_{10}]$ (Gagor *et al.*, 2011), which exhibits a sequence of three phases upon cooling (IPEMAS, IPEMAS01 and IPEMAS02 for phases I–III, respectively) and possesses the smallest *A* cation of these hybrid $Cs_4Mg_3F_{10}$-type compounds, is the most recent. Of note also are the $[(C_6H_5)N(CH_3)_3]_4[Pb_3Br_{10}]$ (Wiest *et al.*, 1999; CAQVIZ) and $[(C_6H_5)N(CH_3)_3]_4[Sn_3I_{10}]$ (Lode & Krautscheid, 2001; RAJMUK) structures, which belong to the $Cs_4Cu_3F_{10}$ structure type. We present here the 100 and 240 K structures of the title compound, $(n\text{-}C_3H_7NH_3)_4[Ni_3Cl_{10}]$, (I), which is the first example of a hybrid $Cs_4Mg_3F_{10}$-type structure containing an open-shell transition metal ion.

Compound (I) remains in the $Cs_4Mg_3F_{10}$ aristotype space group from ambient temperature to 80 K with an undistorted $\{[Ni_3Cl_{10}]^{4-}\}_n$ zigzag layer network, unlike other hybrid structures (at ambient temperature or below) in which neighboring trimetal segments are displaced to give non-

 doi:10.1107/S0108270111050116

rectangular voids between them and lower space-group symmetry. The Ni^{2+} ions of the 2/*m*-symmetric trinickel

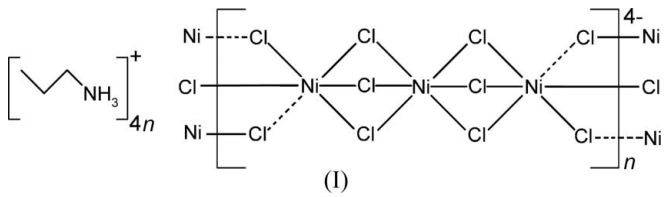

(I)

segment exhibit compressed square–bipyramidal coordination environments. Atoms Cl1 and Cl3 are axial for the terminal atom Ni1, with an average bond length of 2.3734 (3) Å [2.3750 (5) Å at 240 K], *versus* an average equatorial bond length of 2.4539 (2) Å [2.4652 (3) Å at 240 K]. While both axial lengths are less than the equatorial lengths, Ni1—Cl1 is substantially shorter than Ni1—Cl3, since the former is terminal while the latter is bridging. The central Ni2 environment is less compressed, with the difference between the equatorial Ni2—Cl4 and axial Ni2—Cl3 bond lengths equal to 0.0268 (4) Å [0.0324 (7) Å at 240 K]. Atom Cl2 bridges to a neighboring trinickel segment to generate the zigzag layer, with the Ni1—Cl2—$Ni1^{iv}$ bridge [symmetry code: (iv) $x+\frac{1}{2}, y, -z+\frac{1}{2}$] almost linear [164.908 (17)°]; indeed, this is the most linear of the hybrid compounds, where values of 142.51 (3) (WEHSAE), 142.79 (POPHAD), 144.56 (EGUFUI), 153.83 and 154.38 (IPEMAS02), 155.32 (IPEMAS01), 158.42 (IPEMAS) and 159.01 (5)° (IGECIG) are observed. A plot of the trinickel segment with the two non-equivalent *n*-propylammonium cations in (I) is presented in Fig. 1 for the 100 and 240 K structures. Coordination bond lengths and angles are presented in Tables 1 (100 K) and 3 (240 K).

As the first hybrid metal–organic $Cs_4Mg_3F_{10}$-type structure with an open-shell metal cation (d^8, $S = 1$), the magnetic properties of (I) are of interest. Exchange coupling between electron spins on neighboring metal cations in bridged systems depends on, among other factors, the $M-X-M$ bridging angle (Kahn, 1985), with the ferromagnetic (FM) coupling expected at 90° becoming antiferromagnetic (AFM) as the bridge angle deviates from this. Thus, the quasi-linear monobridge between trinickel segments favors AFM coupling. Magnetic susceptibility measurements of linear chain tri-μ-chlorido-bridged $ANiCl_3$ compounds indicate the crossover point from FM to AFM coupling likely occurs close to the bridging angle values (77–79°) within the trinickel segment of (I). In $[(CH_3)_4N][NiCl_3]$, for example, the bridging Cl—Ni—Cl angle is 78.74° (Stucky, 1968) with weak FM coupling (J/k = 1.7 K; Hijmans *et al.*, 1984). The Cs^+, NH_4^+, Rb^+ and Tl^+ salts confirm the trend by showing, respectively, greater AFM coupling correlated with shorter neighboring Ni···Ni distances within the chain and, hence, smaller Ni—Cl—Ni angles (Witteveen & van Veen, 1974). Thus, the coupling within the trinickel segment should be weak (whether AFM or FM), with AFM coupling along the rows of Ni1 atoms at the folds of the zigzag layer (corresponding to the crystallographically sheared slabs derived from the parent K_2NiF_4 structure type) dominant. In contrast, $Cs_4Ni_3F_{10}$ shows spontaneous magnetization in the range 9.5 to 21 K, attributed to strong FM coupling within the trinickel segment similar to that within the $(NiF_3^-)_n$ linear chains of $CsNiF_3$, but AFM ordering below 9.5 K, attributed to weaker coupling between trinuclear segments across the quasi-linear Ni—F—Ni bridges (Schmidt *et al.*, 1992).

The mirror-symmetric propylammonium cations of (I) exhibit staggered conformations but with differences in disorder (although no thermal anomaly is observed between 183 and 313 K). Displacement ellipsoids elongated perpendicular to the mirror plane for C atoms and Cl1 at 100 K suggest dynamic disorder across the plane, although no disorder is present in the model. Such anisotropy is absent at 240 K, but minor disorder components are observed in which the central C-atom conformation is reversed. Given the large area avail-

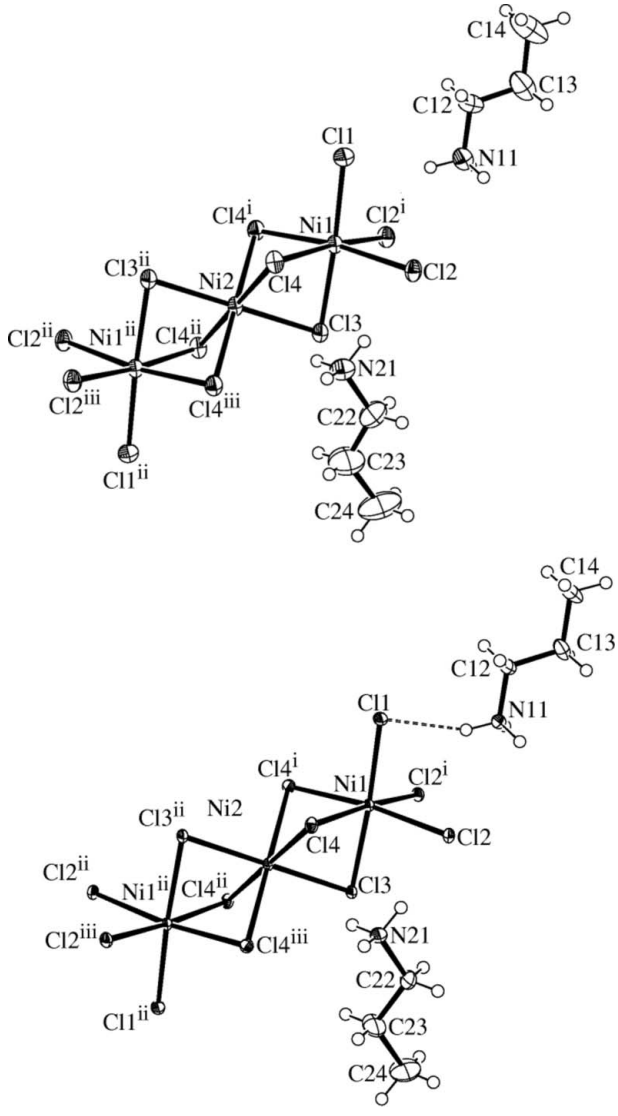

Figure 1
The Ni_3Cl_{12} segment and the two inequivalent cations in (I) at 100 (bottom) and 240 K (top). The minor disorder component at 240 K and one-half of any twofold disordered $-CH_3$ or $-NH_3$ groups have been omitted for clarity. Displacement ellipsoids are drawn at the 50% probability level. [Symmetry codes: (i) $-x, y, z$; (ii) $-x, -y+1, -z$; (iii) $x, -y+1, -z$.]

able to the propylammonium cation, it is not surprising that disorder is present. Four cation head groups in (I) occupy a given side of the inorganic layer demarcated by *a* and *c*, to give an area of 30.0197 (2) Å^2 [30.3798 (3) Å^2 at 240 K] per cation. In comparison, the area occupied per cation on a given side of the inorganic layer in $(n\text{-}C_3H_7NH_3)_2[MnCl_4]$ is only 27–28 Å^2, and this in a system for which cation disorder is a key feature. Ammonium head groups for both cations fit into cages formed by chloride ions of neighboring trinickel segments of the layer: the N11 head group is surrounded by seven close N$\cdots$Cl contacts [3.1536 (13) (Cl1), 3.3451 (11) (Cl4 × 2), 3.4480 (11) (Cl2 × 2) and 3.4649 (1) Å (Cl1 × 2) at 100 K], and the N21 head group by eight close N$\cdots$Cl contacts [3.2677 (11) (Cl4 × 2), 3.3669 (11) (Cl2 × 2), 3.4588 (1) (Cl3 × 2) and 3.6061 (12) Å (Cl4 × 2) at 100 K]. The N atoms are almost on a line between two equivalent Cl ligands of parallel neighboring trinickel segments but are set slightly further into the layer, as shown by the Cl1$^{v}\cdots$N11$\cdots$Cl1^{vi} [172.06 (4)°; symmetry codes: (v) $-x+\frac{1}{2}, y, -z+\frac{1}{2}$; (vi) $-x-\frac{1}{2}, y, -z+\frac{1}{2}$] and Cl3$\cdots$N21$\cdots$Cl3^{vii} [175.88 (5)°; symmetry code: (vii) $x+1, y, z$] angles at 100 K being slightly less than 180°, so as to position the head group to take advantage of these abundant hydrogen-bonding opportunities. The only ordered head group is that of atom N11 at 100 K, where the H atoms link to the Cl atoms with the closest N$\cdots$Cl contacts (Cl1 and Cl4), and for which hydrogen-bond parameters are listed in Table 2.

The *n*-propylammonium cations of (I) form an interdigitated bilayer, interleaved between the inorganic layers, in which methyl groups from both sides are packed together in the middle to provide more efficient use of space than a bilayer in which the terminal groups of the organic cations abut one another. Such a packing arrangement in the center of the bilayer is found for $(n\text{-}C_3H_7NH_3)_2[MnCl_4]$, where it is seen as an important factor in the phase behavior of the system (Depmeier, 2009). However, the zigzag inorganic layer induces a more complicated bilayer structure than that found in a layer perovskite. Cation 1 (N11) is located about the convex folds of the inorganic layer so that the tail groups from cations on one side of the bilayer penetrate further into the opposite side to position terminal atom C14 of one cation slightly past atom C13^{viii} [symmetry code: (viii) $x+\frac{1}{2}, -y+\frac{1}{2}, -z+1$] of the cation on the opposite side. Cations on different sides of the convex fold are related by an *a*-glide operation that positions atoms C13 and C14 as the walls of a groove parallel to *a*. Cations 2 (N21) are located about the concave folds of the inorganic layers with their alkyl tails pointing toward each other, so that terminal atoms C24 act as a tongue that fits in the groove formed by cations 1 on the opposite side. While this description of the bilayer structure is most apparent when viewed along *a*, note that trinickel segments across the fold (and in layers above and below) are staggered relative to each other. As a result, the cations on the opposite walls of the groove are staggered, as are those in the tongue. Since the repeat distance between equivalent cations along *a* is almost 7 Å, the image of a tight-fitting tongue-and-groove is oversimplified. Indeed, a calculation of voids (probe radius = 0.8 Å, grid spacing = 0.1 Å; *MercuryCSD*, Version 2.4; Macrae *et al.*, 2008) finds the only voids (5.588 Å^3 × 4 = 1.6% of unit-cell volume) between neighboring cations 2 in the bilayer. The disposition of the phenylalkyl groups in IGECIG and WEHSAE is similar, although in these cases the voids in the organic bilayer (calculated under the same conditions) occupy a far larger fraction of the unit-cell volume (10–11%) because of the larger spacing required by the larger atoms in the $\{[Pb_3I_{10}]^{4-}\}_n$ layer. The phenylammonium cation disposition in POPHAD and EGUFUI can also be described in this manner with bilayer voids occupying the same unit-cell volume fraction as in (I), although the tongue-and-groove arrangement of these more rigid cations is less defined. The three phases of IPEMAS show void fractions in an intermediate range of 4.2, 3.4 and 3.9% for phases I–III, respectively. Hence, the structure of (I), in which the slender propylammonium cation is paired with the smallest metal cation/halide pair of these hybrid structures, has one of the most efficient organic cation packings of the hybrid $Cs_4Mg_3F_{10}$-type compounds. A packing diagram for (I) at 100 K viewed parallel to *a* to show the interleaved inorganic layers and organic bilayers is presented in Fig. 2.

Compound (I) is similar in many respects to the isomorphous high-temperature phase I of $(i\text{-}C_3H_7NH_3)_4[Cd_3Cl_{10}]$ (IPEMAS). The zigzag inorganic layer here is also undistorted and the two independent organic cations are located at the convex or concave folds of the inorganic layer. However, the isopropyl group is bulky enough that the alkyl tails are not interdigitated. $(n\text{-}C_3H_7NH_3)_8[Pb_5I_{18}]$ (Billing & Lemmerer, 2006*b*; GEHPEP) provides an interesting comparison structure in which the same organic cation as in (I) is found with a more complicated inorganic layer. Here, squares of corner-sharing PbI_6 octahedra, similar to the corner-sharing arrangement in the layer perovskites, form parallel stacks,

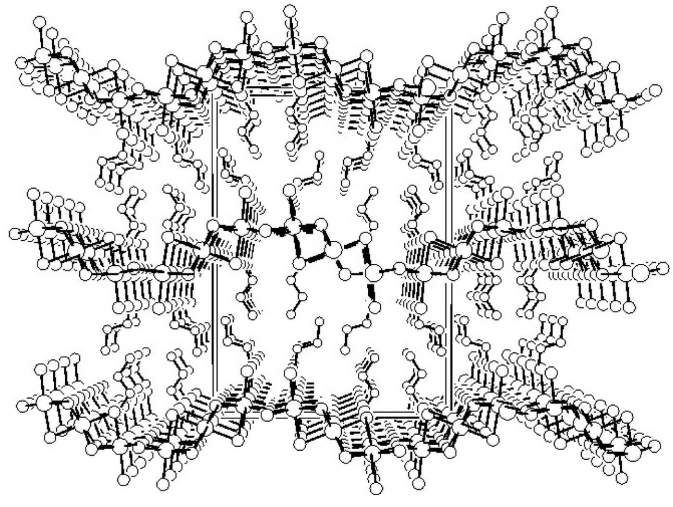

Figure 2
Packing diagram for (I) at 100 K, viewed parallel to *a* (*b* vertical and *c* horizontal), showing the tongue-and-groove interdigitated bilayers of *n*-propylammonium cations interleaved with the zigzag inorganic layers. H atoms have been omitted for clarity. Ni atoms are drawn as large circles, Cl atoms as medium-sized circles, and N and C atoms as small circles.

while Pb_3I_{12} segments of face-sharing PbI_6 octahedra, similar to those found in the $Cs_4Mg_3F_{10}$-type structures, link adjacent stacks. Three of the eight unique n-$C_3H_7NH_3^+$ cations in GEHPEP do exhibit disorder similar to that reported here for the 240 K structure of (I), although with a lower occupancy for the major component (54–60%).

Experimental

(n-$C_3H_7NH_3$)Cl (5.0 g) was dissolved with $NiCl_2{\cdot}6H_2O$ at a 2:1 molar ratio in 6 *M* HCl (40 ml) and the solution maintained at 333 (5) K until a dark-red solid formed upon evaporation. Crystals of (I) cut from the solid mass are orange in color. Thermal analysis was performed using a TA Instruments Q200 DSC cooled by an RCS refrigeration system with a crystalline sample mass of 4.8 mg ramped between 183 and 313 K at a rate of 5.00 K min^{-1}.

Compound (I) at 100 K

Crystal data

$(C_3H_{10}N)_4[Ni_3Cl_{10}]$
M_r = 771.09
Orthorhombic, *Cmce*
a = 6.9132 (1) Å
b = 23.9825 (2) Å
c = 17.3695 (2) Å
V = 2879.79 (6) Å^3
Z = 4
Mo $K\alpha$ radiation
μ = 2.88 mm^{-1}
T = 100 K
0.25 × 0.19 × 0.16 mm

Data collection

Nonius KappaCCD area-detector diffractometer
Absorption correction: multi-scan (*DENZO* and *SCALEPACK*; Otwinowski & Minor, 1997)
T_{min} = 0.527, T_{max} = 0.638
3904 measured reflections
3904 independent reflections
3435 reflections with $I > 2\sigma(I)$
R_{int} = 0.043

Refinement

$R[F^2 > 2\sigma(F^2)]$ = 0.023
$wR(F^2)$ = 0.056
S = 1.03
3904 reflections
85 parameters
H-atom parameters constrained
$\Delta\rho_{max}$ = 0.70 e Å^{-3}
$\Delta\rho_{min}$ = −1.10 e Å^{-3}

Compound (I) at 240 K

Crystal data

$(C_3H_{10}N)_4[Ni_3Cl_{10}]$
M_r = 771.09
Orthorhombic, *Cmce*
a = 6.9786 (1) Å
b = 24.0608 (5) Å
c = 17.4131 (3) Å
V = 2923.85 (9) Å^3
Z = 4
Mo $K\alpha$ radiation
μ = 2.84 mm^{-1}
T = 240 K
0.25 × 0.19 × 0.16 mm

Data collection

Nonius KappaCCD area-detector diffractometer
Absorption correction: multi-scan (*DENZO* and *SCALEPACK*; Otwinowski & Minor, 1997)
T_{min} = 0.540, T_{max} = 0.646
3960 measured reflections
3960 independent reflections
2216 reflections with $I > 2\sigma(I)$
R_{int} = 0.094

Refinement

$R[F^2 > 2\sigma(F^2)]$ = 0.038
$wR(F^2)$ = 0.088
S = 1.00
3960 reflections
97 parameters
6 restraints
H-atom parameters constrained
$\Delta\rho_{max}$ = 0.72 e Å^{-3}
$\Delta\rho_{min}$ = −1.30 e Å^{-3}

Table 1
Selected geometric parameters (Å, °) for (I) at 100 K.

Ni1—Cl1	2.3325 (4)	Ni1—Cl4	2.4473 (3)
Ni1—Cl2	2.4604 (1)	Ni2—Cl3	2.3853 (3)
Ni1—Cl3	2.4142 (4)	Ni2—Cl4	2.4121 (2)
Cl1—Ni1—Cl2	93.482 (11)	Cl3—Ni1—Cl4	84.537 (9)
Cl1—Ni1—Cl3	176.187 (14)	Cl4—Ni1—Cl4^{i}	83.927 (12)
Cl1—Ni1—Cl4	92.633 (10)	Cl3—Ni2—Cl4	85.937 (8)
Cl2—Ni1—Cl2^{i}	89.247 (6)	Cl4—Ni2—Cl4^{ii}	94.563 (12)
Cl2—Ni1—Cl3	89.230 (10)	Ni1—Cl2—Ni1^{iv}	164.908 (17)
Cl2—Ni1—Cl4	93.084 (6)	Ni2—Cl3—Ni1	78.144 (10)
Cl2—Ni1—Cl4^{i}	173.311 (11)	Ni2—Cl4—Ni1	77.001 (8)

Symmetry codes: (i) $-x, y, z$; (ii) $x, -y+1, -z$; (iv) $x+\frac{1}{2}, y, -z+\frac{1}{2}$.

Table 2
Hydrogen-bond geometry (Å, °) for (I) at 100 K.

100 K

D—H···A	D—H	H···A	D···A	D—H···A
N11—H11A···Cl1	0.89	2.31	3.1536 (13)	158
N11—H11B···Cl4^{iv}	0.89	2.54	3.3451 (10)	150

Symmetry code: (iv) $-x+\frac{1}{2}, y, -z+\frac{1}{2}$.

Table 3
Selected geometric parameters (Å, °) for (I) at 240 K.

Ni1—Cl1	2.3299 (8)	Ni1—Cl4	2.4580 (5)
Ni1—Cl2	2.4724 (2)	Ni2—Cl3	2.3869 (6)
Ni1—Cl3	2.4200 (7)	Ni2—Cl4	2.4193 (4)
Cl1—Ni1—Cl2	93.44 (2)	Cl3—Ni1—Cl4	84.136 (17)
Cl1—Ni1—Cl3	176.56 (3)	Cl4—Ni1—Cl4^{i}	83.76 (2)
Cl1—Ni1—Cl4	93.308 (18)	Cl3—Ni2—Cl4	85.691 (16)
Cl2—Ni1—Cl2^{i}	89.765 (11)	Cl4—Ni2—Cl4^{ii}	94.59 (2)
Cl2—Ni1—Cl3	89.00 (2)	Ni1—Cl2—Ni1^{iv}	164.34 (4)
Cl2—Ni1—Cl4	92.840 (11)	Ni1—Cl3—Ni2	78.62 (2)
Cl2—Ni1—Cl4^{i}	172.61 (2)	Ni1—Cl4—Ni2	77.270 (15)

Symmetry codes: (i) $-x, y, z$; (ii) $x, -y+1, -z$; (iv) $x+\frac{1}{2}, y, -z+\frac{1}{2}$.

A series of structures were determined from ambient temperature to 80 K. Since the details of the 80, 100 and 120 K structures agree with only minor differences, the structure at 100 K alone is reported here. Likewise, the details of the 210, 240 K and ambient-temperature structures agree, including disorder of the *n*-propyl chains, so the 240 K structure alone is reported here.

H-atom positions were calculated using a riding model, with methyl C—H = 0.96 Å, methylene C—H = 0.97 Å and ammonium N—H = 0.89 Å, with twofold disorder of –NH_3 and –CH_3 groups, and with U_{iso}(H) = 1.5U_{eq}(C,N). Bond lengths and angles within the organic cations conform to expected values (Ladd & Palmer, 1994). Low-angle reflections obscured by the beamstop (as indicated by $F_o^2 << F_c^2$) were omitted from the refinement. Exceptions and details for the 100 and 240 K structures follow.

At 100 K, atom Cl1 and some of the C atoms exhibit elongated displacement ellipsoids parallel to *a*, suggesting disorder about the mirror plane. However, *SHELXL97* (Sheldrick, 2008) did not recommend splitting the atom sites, and refinement of a disordered model only gave a modest improvement in *R* factors (wR = 0.051 against 104 parameters). Solution and refinement in the noncentrosymmetric space group *C*2*ce* yielded similar elongation of displace-

ment ellipsoids. Hence, the ordered centrosymmetric model was retained. H atoms bound to N11 were calculated without disorder.

At 240 K, difference-map peaks near the central atoms, C*X*2 and C*X*3, of the propylammonium cations indicate a minor disordered component in which the orientation of these atoms is flipped. A common site-occupation factor [0.232 (8) for cation 1 and 0.128 (9) for cation 2] and a common isotropic displacement parameter were refined for the minor-conformation C*X*2 and C*X*3 atoms in each propylammonium chain. C—N and C—C bond lengths within the minor components were restrained loosely to 1.50 (2) Å.

For both temperatures, data collection: *COLLECT* (Nonius, 1998); cell refinement: *SCALEPACK* (Otwinowski & Minor, 1997); data reduction: *DENZO* (Otwinowski & Minor, 1997) and *SCALEPACK*; program(s) used to solve structure: *SIR92* (Altomare *et al.*, 1993); program(s) used to refine structure: *SHELXL97* (Sheldrick, 2008); molecular graphics: *ORTEP-3 for Windows* (Farrugia, 1997); software used to prepare material for publication: *WinGX* (Farrugia, 1999).

The authors thank the National Science Foundation DUE CCLI–A&I program (grant No. 9951348) and Southeast Missouri State University for funding the X-ray diffraction facility.

Supplementary data for this paper are available from the IUCr electronic archives (Reference: FG3235). Services for accessing these data are described at the back of the journal.

References

Allen, F. H. (2002). *Acta Cryst.* B**58**, 380–388.
Altomare, A., Cascarano, G., Giacovazzo, C. & Guagliardi, A. (1993). *J. Appl. Cryst.* **26**, 343–350.
Bertheville, B., Fischer, P. & Yvon, K. (2002). *J. Alloys Compd*, **330–332**, 152–156.
Billing, D. G. & Lemmerer, A. (2006*a*). *Acta Cryst.* C**62**, m174–m176.
Billing, D. G. & Lemmerer, A. (2006*b*). *Acta Cryst.* C**62**, m238–m240.
Blattner, H., Gränicher, H., Känzig, W. & Merz, W. (1948). *Helv. Phys. Acta*, **21**, 341–354.
Carim, A. H., Dera, P., Finger, L. W., Mysen, B., Prewitt, C. T. & Schlom, D. G. (2000). *J. Solid State Chem.* **149**, 137–142.
Costin-Hogan, C. E., Chen, C.-L., Hughes, E., Pickett, A., Valencia, R., Rath, N. P. & Beatty, A. M. (2008). *CrystEngComm*, **10**, 1910–1915.
Depmeier, W. (2009). *Z. Kristallogr.* **224**, 287–294.
Dussarrat, C., Grasset, F., Bontchev, R. & Darriet, J. (1996). *J. Alloys Compd*, **233**, 15–22.
Dussarrat, C., Grasset, F. & Darriet, J. (1995). *Eur. J. Solid State Inorg. Chem.* **32**, 557–576.
Farrugia, L. J. (1997). *J. Appl. Cryst.* **30**, 565.
Farrugia, L. J. (1999). *J. Appl. Cryst.* **32**, 837–838.
Floros, N., Hervieu, M., van Tendeloo, G., Michel, C., Maignan, A. & Raveau, B. (2000). *Solid State Sci.* **2**, 1–9.
Gagor, A., Waśkowska, A., Czapla, Z. & Dacko, S. (2011). *Acta Cryst.* B**67**, 122–129.
Hijmans, T. W., van Duyneveldt, A. J. & de Jongh, L. J. (1984). *Physica B*, **125**, 21–32.
Ishihara, H., Krishnan, V. G., Dou, S., Paulus, H. & Weiss, A. (1994). *Z. Naturforsch. Teil A*, **49**, 213–222.
Kahn, O. (1985). *Magneto-Structural Correlations in Exchange Coupled Systems*, edited by R. D. Willett, D. Gatteschi & O. Kahn, pp. 37–56. Dordrecht: Reidel.
Kissel, D. & Hoppe, R. (1988). *Z. Anorg. Allg. Chem.* **561**, 12–24.
Ladd, M. F. C. & Palmer, R. A. (1994). *Structure Determination by X-ray Crystallography*, 3rd ed., pp. 434–435. New York: Plenum Press.
Lode, C. & Krautscheid, H. (2001). *Z. Anorg. Allg. Chem.* **627**, 1454–1458.
Macrae, C. F., Bruno, I. J., Chisholm, J. A., Edgington, P. R., McCabe, P., Pidcock, E., Rodriguez-Monge, L., Taylor, R., van de Streek, J. & Wood, P. A. (2008). *J. Appl. Cryst.* **41**, 466–470.
Maxcy, K. R. & Willett, R. D. (2004). *Encyclopedia of Supramolecular Chemistry*, edited by J. L. Atwood & J. W. Steed, pp. 1387–1393. New York: Marcel Dekker Inc.
Mitzi, D. B. (2004). *Functional Hybrid Materials*, edited by P. Gómez-Romero & C. Sanchez, pp. 347–386. Weinheim: Wiley-VCH.
Mitzi, D. B., Chondroudis, K. & Kagan, C. R. (2001). *IBM J. Res. Dev.* **45**, 29–46.
Müller-Buschbaum, Hk. & Neubacher, M. (1990). *Z. Anorg. Allg. Chem.* **586**, 87–92.
Neubacher, M. & Müller-Buschbaum, Hk. (1991). *Z. Anorg. Allg. Chem.* **594**, 133–138.
Nonius (1998). *COLLECT*. Nonius BV, Delft, The Netherlands.
Otwinowski, Z. & Minor, W. (1997). *Methods in Enzymology*, Vol. 276, *Macromolecular Crystallography*, Part A, edited by C. W. Carter Jr & R. M. Sweet, pp. 307–326. New York: Academic Press.
Raptopoulou, C. P., Terzis, A., Mousdis, G. A. & Papavassiliou, G. C. (2002). *Z. Naturforsch. Teil B*, **57**, 645–650.
Schmidt, R. E., Pebler, J. & Babel, D. (1992). *Eur. J. Solid State Inorg. Chem.* **29**, 679–690.
Sheldrick, G. M. (2008). *Acta Cryst.* A**64**, 112–122.
Steinfink, H. & Brunton, G. (1969). *Inorg. Chem.* **8**, 1665–1668.
Stucky, G. D. (1968). *Acta Cryst.* B**24**, 330–337.
Wiest, Th., Blachnik, R. & Reuter, H. (1999). *Z. Naturforsch. Teil B*, **54**, 1099–1102.
Wilkens, J. & Müller-Buschbaum, Hk. (1991). *Z. Anorg. Allg. Chem.* **592**, 79–83.
Witteveen, H. T. & van Veen, J. A. R. (1974). *J. Phys. Chem. Solids*, **35**, 337–346.